THE IMPACTS OF MULTI-LAG MOMENT PROCESSOR ON A SOLID-STATE POLARIMETRIC WEATHER RADAR

B. L. Cheong[1,2,*], J. M. Kurdzo[1,3], G. Zhang[1,3] and R. D. Palmer[1,3]

[1] Advanced Radar Research Center, University of Oklahoma, Norman, OK, U.S.A.
[2] School of Electrical and Computer Engineering, University of Oklahoma, Norman, OK, U.S.A.
[3] School of Meteorology, University of Oklahoma, Norman, OK, U.S.A.

Abstract

Solid-state weather radars generally require pulse compression and blind range mitigation waveforms in order to gain sufficient sensitivity due to the low peak power of transmitters and mitigate the near-range data loss due to the long transmit duty cycle, respectively. At the Advanced Radar Research Center (ARRC) of the University of Oklahoma, we have developed a solid-state polarimetric weather radar, the PX-1000, which uses a long waveform for far range observations and short waveform for blind range filling. It should be emphasized here that we typically use a virtually non-tapered waveform, which fully utilizes the capacity of the solid-state transmitters. One of the consequences of data acquisition using long and short waveforms is the abrupt change of signal-to-noise ratio (SNR) at the transition range from short waveform to long waveform. This effect is manifested into a discontinuity of cross-pol correlation coefficients ($\rho_{\rm hv}$) in range, which makes subsequent data processing, e.g., data interpretation, automated hydrometeor classification and data assimilation in numerical weather prediction models, more challenging. The multi-mag moment processor, recently developed in the ARRC, is less sensitive to SNR due to its underlying concept of fitting the auto- and cross-correlation estimates to the Gaussian functions without using the auto-correlation estimates at lag-0. In addition, this algorithm does not depend on noise estimation because the use of lag-0 auto-correlation is avoided. In this work, we focus on the $\rho_{\rm hv}$ estimation. We found that the multi-lag moment processor provides superior results in $\rho_{\rm hv}$ estimates compared to the canonical method, especially when the SNR is moderate to low (< 20 dB), which is most typical for low-power solid-state weather radars. Several cases will be presented to illustrate the impacts on $\rho_{\rm hv}$.

1. BACKGROUND

Correlation coefficient $\rho_{\rm hv}$ is a measure of the degrees of similarity between the two polarizations, which is related to size, shape and composition of hydrometeors. It is one of the key components in the hydrometeor classification algorithm (HCA) (Park et al., 2009; Zrnić et al., 2001), which is a fuzzy-logic based method that uses 6 radar variables, i.e., (1) reflectivity from the horizontal channel Z, (2) differential reflectivity, (3) cross-correlation coefficient, (4) specific differential phase $K_{\rm DP}$, (5) a texture ${\rm SD}(Z)$ derived from Z, and (6) a texture ${\rm SD}(\phi_{\rm DP})$ derived from $\phi_{\rm DP}$, to produce hydrometeor classes. It has been reported that $\rho_{\rm hv}$ can be used to predict signal quality and gauge hail size (Balakrishnan and Zrnić, 1990). Correlation coefficient $\rho_{\rm hv}$ can also be used to discriminate rain and wet snow as signal correlation decreases when particles are wet or irregular in shape (Straka et al., 2000). That is, one can get an accurate assessment of whether the precipitation contains wet snow by inspecting the $\rho_{\rm hv}$ values as wet snow typically has $\rho_{\rm hv}$ that are lower than that of rain. The $\rho_{\rm hv}$ estimate also plays an important role in methods to distinguish meteorological against non-meteorological echoes, e.g., birds, insects and smoke (Tang et al., 2013).

At X-band, the output power produced by solid-state amplifiers is still relatively low, on the orders of 100's of watts, and, thus, the returned signals often have moderate to low SNR. As $\rho_{\rm hv}$ degrades with decreasing SNR (Bringi and Chandrasekar, 2001), one can expect that the quality of $\rho_{\rm hv}$ is widely degraded on an X-band solid-state weather radar. The primary motivation of this work is to explore the impacts of the multilag moment processor, which promises improved performance at low SNR regimes that are typically found with solid-state weather radars.

1.1. Signal Processing Method

Using the PX-1000, an ARRC in-house-developed 100-W solid-state X-band polarimetric weather radar, raw time series data consisting of digitized in-phase and quadrature (IQ) components are used to derive radar moments and polarimetric variables. The radar uses pulse compression with a time-frequency multiplexed (TFM) waveform to eliminate the blind range due to the use of long transmit cycle (Cheong et al., 2013). The transmit cycle is approximately 10 km in the results that will be presented in this article. Briefly, the transmit waveform is a time multiplex of a long waveform and a short waveform, i.e., a temporal concatenation. The short waveform is appended to the end of the long waveform in this order in order for the technique to be viable as the total blind range is the sum of the two pulse lengths. The two waveforms use two distinct bands that do not overlap each other.

* *Corresponding author address:* Boon Leng Cheong, University of Oklahoma, Advanced Radar Research Center, 120 David L. Boren Blvd., Rm 4640, Norman, OK 73072-7307; e-mail: boonleng@ou.edu

One can also think of the short waveform as a second virtual radar operating synchronously with a slight delay (duration of the long pulse). The IQ time series are de-multiplexed on the signal processor through two match filters that separate the signals from each other.

Figure 1 shows the theoretical radar sensitivity in range with the minimum detectable signal (MDS) assumed at SNR at 0 dB. The two sensitivity curves of the PX-1000 are shown at ranges where they are applicable. A CASA IP-1 X-band (McLaughlin et al., 2009; Brotzge et al., 2006) is included for reference as they have numerous system specifications in common. As indicated in the chart, the abrupt change in sensitivity of 15 dB at 10 km can be expected for the radar reflectivity derived from the TFM waveform of these sub-waveforms. The long waveform (67 μs) has a blind range of 10 km and it is filled with the short waveform (2 μs). Since mid-2012, we have developed an optimized frequency modulation (OFM) scheme, which is a non-linear frequency modulation derived from an iterative optimization algorithm (Kurdzo et al., 2014), and it has been applied to the TFM waveform. Figure 1 shows the updated sensitivity profile. Due to the limitations of receiver bandwidth, we are unable to match the range resolution of the two waveforms but they are close and do not impede the assessments drawn in this study. As one can readily see from the chart, the radar is capable of observing rain ($>$ 20 dBZ) up to 60 km away. It should be noted, however, that the SNR of typical precipitation events at 20 dBZ just barely exceed the MDS threshold at the outer ranges, i.e., 10 km of the short pulse and 60 km of the long pulse, along with the just mentioned abrupt change.

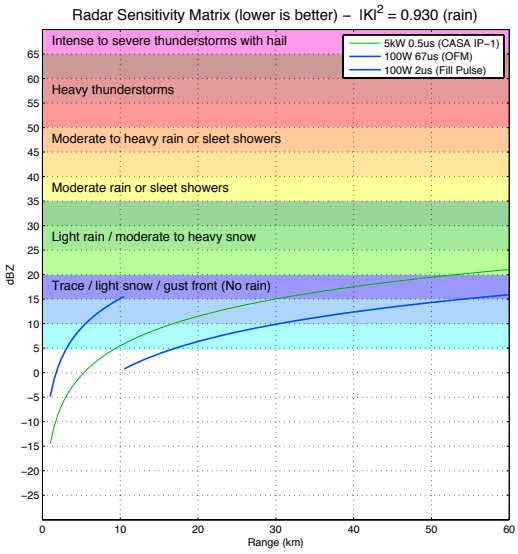

Figure 1: Radar sensitivity of the PX-1000.

1.2. Multilag Estimator

In this study, the multilag moment estimator (Lei et al., 2012) was implemented on the real-time signal processor of the PX-1000 radar. The algorithm uses a Gaussian model as a fitting function to the autocorrelation function, which can be described mathematically as

$$R(mT_s) = S\rho(mT_s)\exp(-\frac{j\pi m\bar{v}}{v_N}) + N\delta(m), \quad (1)$$

where m represents the digital sample index, T_s represents the sampling time interval, S represents the signal power, ρ represents the true autocorrelation of the signals, $\bar{v}$ represents the mean velocity, v_N represents the Nyquist velocity and N represents the system noise. Similarly, the cross-correlation function is modeled as

$$C(mT_s) = \sqrt{S_h S_v}\rho_{\rm hv}\rho(mT_s)\exp\left[-j(\frac{\pi m\bar{v}}{v_N} + \phi_{\rm dp})\right], \quad (2)$$

where S_h and S_v represent the signal from horizontal and vertical channels, respectively, $\rho_{\rm hv}$ represents the cross-correlation, and $\phi_{\rm dp}$ represents the differential phase.

A series of detailed derivations was presented by Lei et al. (2012) to obtain the estimators in various lags for all the base moments and polarimetric variables. The lag-3 estimators, which is used throughout the study, are included here for convenient reference. The signal power and cross-correlation estimates are computed as

$$\hat{S} = \frac{|\hat{R}(T_s)|^{\frac{6}{7}}||\hat{R}(2T_s)|^{\frac{3}{7}}}{|\hat{R}(3T_s)|^{\frac{3}{7}}}, \quad (3)$$

$$\hat{\rho_{\rm hv}} = |\hat{C}^{(3)}| \times \frac{[|\hat{R}_{\rm h}(3T_s)||\hat{R}_{\rm v}(3T_s)|]^{\frac{1}{7}}}{[|\hat{R}_{\rm h}(T_s)||\hat{R}_{\rm v}(T_s)|]^{\frac{3}{7}}[|\hat{R}_{\rm h}(2T_s)||\hat{R}_{\rm v}(2T_s)|]^{\frac{3}{14}}} \quad (4)$$

where $|C^{(3)}|$ is the cross-correlation fitting using lags up to $3T_s$ and its general form is described as

$$|C^{(N)}| = \exp\left[\frac{3\sum_{m=-N}^{N}\alpha(m)\ln|\hat{C}(mT_s)|}{(2N-1)(2N+1)(2N+3)}\right] \quad (5)$$

where $\alpha(m) = (3N^2 + 3N - 1 - 5m^2)$, and $\hat{C}(mT_s)$ is the conventional cross-correlation estimate.

Figure 2 illustrates an example of fitting Gaussian functions to a set of correlation coefficients derived from raw data at different lags. One can see that the lag-0 estimate is clearly contaminated by white noise and it is not used by the multilag estimator.

2. PRELIMINARY RESULTS

Three case studies will be presented to illustrate the impacts of multilag moment processor on various conditions. They

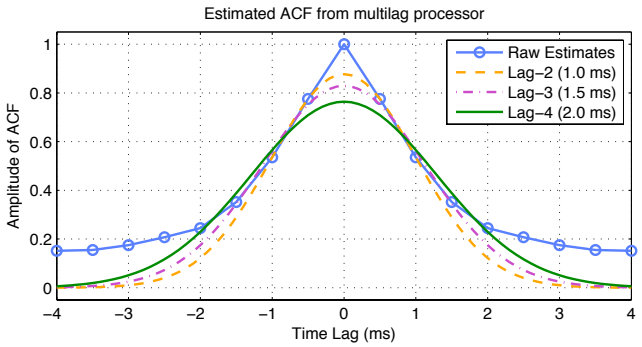

Figure 2: An example illustrating the fitted Gaussian function using different number of lag estimates.

include a stratiform rain case, a squall line with a gust front which featured biological targets, and a winter precipitation case with rain and wet snow.

2.1. Case 1: Stratiform Rain

A dataset on 2013/06/17 09:58 UTC from the PX-1000 along with the closest scan from the KTLX, which is an operational WSR-88D radar, are shown in Figure 3 for comparison. The KTLX data are used for comparison as it is well calibrated and the data within the domain of interest, i.e., within 60 km range of the PX-1000, are of high SNR.

At this time, stratiform rain was observed within the radar domain and reflectivity and high values of $\rho_{\rm hv}$ can be seen to be homogeneous throughout the domain of interest. The same radar variables from the PX-1000, shown in the lower four panels, are derived using the conventional processing method, i.e., canonical correlation estimate (the middle two panels) and the multilag processing method (the lowest 2 panels). Besides the two missing sectors because of blockages, i.e., one due south and one due north-east, the reflectivity fields are in good agreements. Some attenuation through rain for the X-band PX-1000 is expected as the radar wavelength is shorter, which is more susceptible in that regard. Within the scope of discussion, the rain attenuation is not corrected.

Near the 10 km range, which is right outside of the blind range, high values of $\rho_{\rm hv}$ estimate can be seen from all processing methods and the KTLX data. With pulse compression, a moderate SNR of 20 dB from a 20 dBZ echo at this range can be expected for the PX-1000 radar (Figure 1). As expected, the $\rho_{\rm hv}$ field can be seen to suffer degradation due to the SNR decrease as range increases. Usable $\rho_{\rm hv}$ is very limited due to this degradation. In addition, an abrupt transition in $\rho_{\rm hv}$ at 10 km range can be seen from the right panels of the middle row, due to the waveform switch as mentioned previously. By using the multilag cross-correlation estimate in Eq. (4), the sensitivity of $\rho_{\rm hv}$ estimate is virtually eliminated as shown in the lower right panel of Figure 3. The $\rho_{\rm hv}$ field is similar to the data from the KTLX even at the outer of range of the radar domain.

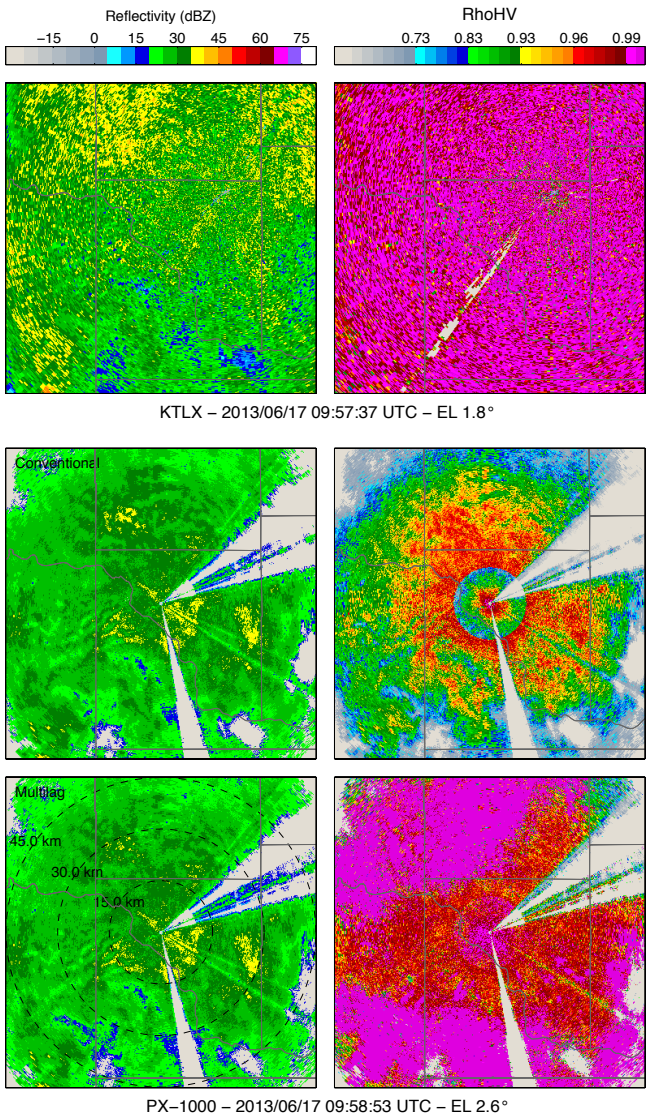

Figure 3: Comparisons of radar reflectivity and correlation coefficients $\rho_{\rm hv}$ between the KTLX (top row) and the PX-1000 (bottom two rows). Data shown in the middle row are derived using conventional estimation technique and data shown in the bottom row are derived using the lag-3 multilag moment estimator. It is evident that $\rho_{\rm hv}$ suffers degradation due to SNR loss but the multilag method virtually eliminate this degradation.

2.2. Case 2: Squall Line and Biological Targets

A dataset on 2013/06/17 07:55 from the PX-1000 is shown in Figure 4. Very intense precipitation can be seen right along the squall line. Severe attenuation through the squall line

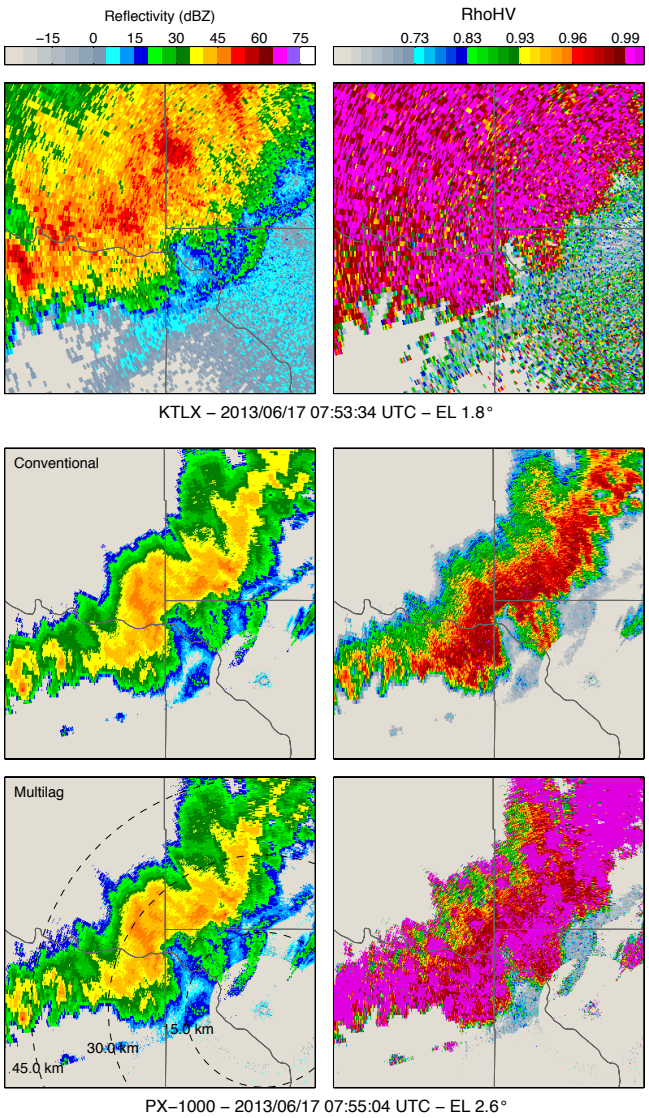

Figure 4: An example data with biological clutter ahead of a squall line. It is clear in this example that the multilag method does not simply scale the ρ_{hv} estimates everywhere in the radar domain but also preserves the low values where signals are not highly correlated.

can be observed in the PX-1000 data and signal extinction can be seen to occur at around 35 km range. Near the fringe of signal extinction, SNR is expected to be low and, thus, the ρ_{hv} estimate suffers degradation as seen in the results from the conventional moment processor. Once again, the multilag estimator successfully eliminates the degradation due to SNR loss and can be seen to maintain high values of ρ_{hv} even near the regions of extremely low SNR.

Within the squall line, ρ_{hv} values exhibit a noisy field in the KTLX data, which may be an indicator of the mix of rain and non-meteorological returns. This is consistent with the ρ_{hv} field from the PX-1000 using the multilag moment processor. In contrast, the signature is completely masked away by the low SNR degradation from the result using the conventional method.

Another interesting observation in this dataset is the biological target signatures ahead of the squall line, which can be seen as weak echoes, 5-20 dBZ in the reflectivity field and low correlation coefficient, $\rho_{\mathrm{hv}} < 0.7$. It is important to note that the multilag method does not simply enhance the value everywhere in the radar domain but retains the unbiased ρ_{hv} of the signals, as shown here. It is clear from this example that algorithms such as the HCA would have difficulties distinguishing biological clutter from the meteorological returns.

2.3. Case 3: Winter Precipitation

A winter dataset on 2013/04/23 23:58 UTC from the PX-1000 is shown in Figure 5. Reflectivity fields are consistent among radars and processing methods as expected. A band of low ρ_{hv} observed in the KTLX data can be seen in the western regions of the radar domain. Note that the location of KTLX is not at the center of this plot so only a partial ring-like band is shown in the KTLX data. A similar band of low ρ_{hv} can also be seen in the correlation coefficient field from the PX-1000 radar using the multilag method. The band of low ρ_{hv} is at closer range of the PX-1000 as the scan elevation is slightly higher (1.5° vs. 2.6°). At 2.6° elevation and 30 km range, this band of low ρ_{hv} indicates the height of the melting layer at approximately 1.36 km, as ρ_{hv} decreases due to the mix of rain and snow.

It is evident that the melting layer is extremely difficult to locate in this case using conventional processing methods as the decrease of ρ_{hv} estimate due to hydrometeor mixing coincides with the decrease in SNR, which degrades the ρ_{hv} as range increases. Automated algorithms such as the HCA would not be able to properly classify the hydrometeor species in such a situation. The multilag processing method is undoubtedly important for solid-state radars that operate at these SNR regimes.

3. CONCLUSIONS AND UPCOMING WORK

Three cases have been presented to illustrate the quality of ρ_{hv} estimates from a 100 W solid-state weather radar using conventional and multilag processing methods. While a pulse compression technique has been utilized to compensate the low peak power of the transmitters, the expected SNR within the radar domain is still generally moderate and/or low. A moment processor such as the multilag method is necessary for solid-state weather radar to be viable as ρ_{hv} estimates are far less sensitive to the SNR of radar signals.

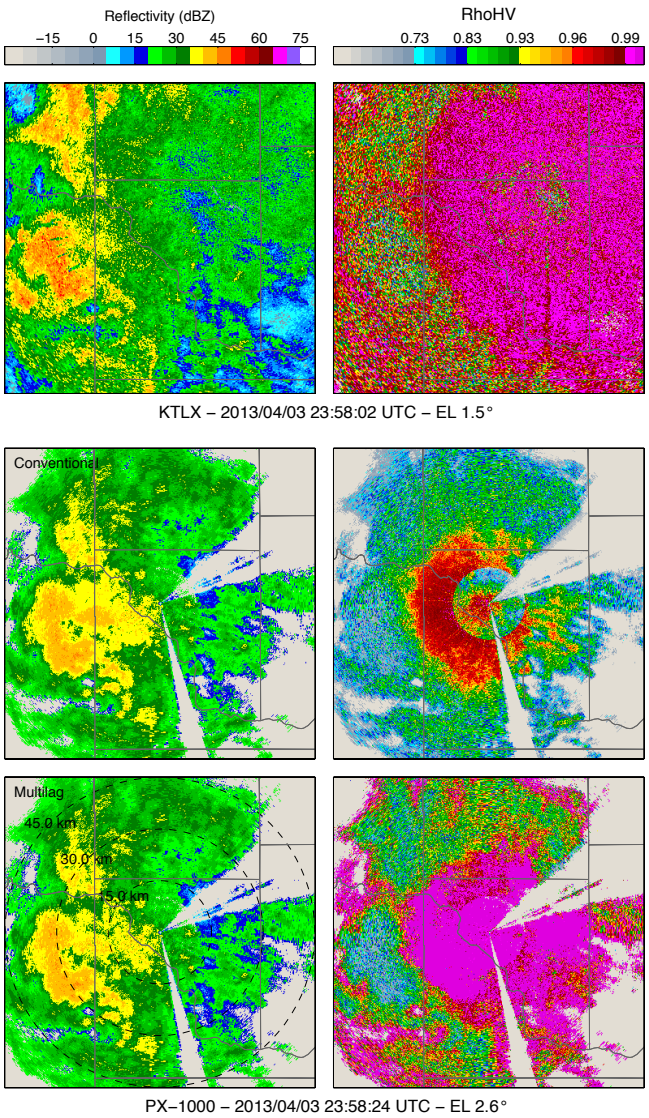

Figure 5: An example data where ρ_{hv} is low at the melting layer. Using conventional processing method would make detection of such signature extremely difficult.

In the near future, an automated HCA would be implemented for the PX-1000 to quantify the impacts of multilag processing method on the HCA for the cases presented in this paper.

ACKNOWLEDGMENT

This work was partially supported by WeatherLink, Inc., Korea.

References

Balakrishnan, N., and D. S. Zrnić, 1990: Use of polarization to characterize precipitation and discriminate large hail. *J. Atmos. Sci.*, **47**, 1525–1540.

Bringi, V. N., and V. Chandrasekar, 2001: *Polarimetric Doppler Weather Radar: Principles and Applications*. Cambridge University Press.

Brotzge, J. A., K. K. Droegemeier, and D. J. McLaughlin, 2006: Collaborative Adaptive Sensing of the Atmosphere (CASA): New radar system for improving analysis and forecasting of surface weather conditions. *J. Transport. Res. Board*, **1948**, 145–151.

Cheong, B. L., R. Kelley, R. D. Palmer, Y. Zhang, and T.-Y. Yu, 2013: PX-1000: A solid-state polarimetric X-band radar and time-frequency multiplexed waveform for blind range mitigation. *IEEE Trans. Instrum. Meas.*, **in press**.

Kurdzo, J. M., B. L. Cheong, R. D. Palmer, G. Zhang, and J. B. Meier, 2014: Pulse compression for high-sensitivity weather radar observations. *J. Atmos. Oceanic Technol.*, **submitted**.

Lei, L., G. Zhang, R. J. Doviak, R. Palmer, B. L. Cheong, M. Xue, Q. Cao, and Y. Li, 2012: Multilag correlation estimators for polarimetric radar measurements in the presence of noise. *J. Atmos. Oceanic Technol.*, **29**(6), 772–795.

McLaughlin, D., D. Pepyne, B. Philips, J. Kurose, M. Zink, D. Westbrook, E. Lyons, E. Knapp, A. Hopf, A. Defonzo, R. Contreras, T. Djaferis, E. Insanic, S. Frasier, V. Chandrasekar, F. Junyent, N. Bharadwaj, Y. Wang, Y. Liu, B. Dolan, K. Droegemeier, J. Brotzge, M. Xue, K. Kloesel, K. Brewster, F. Carr, S. Cruz-Pol, K. Hondl, and P. Kollias, 2009: Short-wavelength technology and the potential for distributed networks of small radar systems. *Bull. Amer. Meteor. Soc.*, **90**(12), 1797–1817.

Park, H., A. V. Ryzhkov, D. S. Zrnić, and K.-E. Kim, 2009: The hydrometeor classification algorithm for the polarimetric WSR-88D: Description and application to an MCS. *Wea. Forecasting*, **24**, 730–748.

Straka, J. M., D. S. Zrnić, and A. V. Ryzhkov, 2000: Bulk hydrometeor classification and quantification using polarimetric radar data: Synthesis of relations. *J. Appl. Meteorol.*, **39**, 1341–1372.

Tang, L., J. Zhang, C. Langston, J. Krause, , K. Howard, and V. Lakshmanan, 2013: A multi-sensor physically based weather/non-weather radar echo classifier using polarimetric and environmental data in a real-time national system. *J. Atmos. Oceanic Technol.*, **under review**.

Zrnić, D. S., A. Ryzhkov, J. Straka, Y. Liu, and J. Vivekanandan, 2001: Testing a procedure for automatic classification of hydrometeor types. *J. Atmos. Oceanic Technol.*, **18**, 892–913.